




## Diatom response to alterations in upwelling and nutrient dynamics associated with climate forcing in the California Current System

Ivia Closset <sup>1\*</sup>, Heather M. McNair <sup>1,2</sup>, Mark A. Brzezinski<sup>1,3</sup>, Jeffrey W. Krause <sup>4,5</sup>, Kimberlee Thamatrakoln<sup>6</sup>, Janice L. Jones<sup>1</sup>

<sup>1</sup>Marine Science Institute, University of California Santa Barbara, Santa Barbara, California

<sup>2</sup>Graduate School of Oceanography, University of Rhode Island, Narragansett, Rhode Island

<sup>3</sup>Department of Ecology Evolution and Marine Biology, University of California, Santa Barbara, California

<sup>4</sup>Dauphin Island Sea Lab, Dauphin Island, Alabama

<sup>5</sup>Department of Marine Sciences, University of South Alabama, Mobile, Alabama

<sup>6</sup>Department of Marine and Coastal Sciences, Rutgers University, New Brunswick, New Jersey

### Abstract

The California Current System displays a strong seasonal cycle in water properties, circulation, and biological production. Interactions of the alongshore current with coastal and topographic features lead to high spatial variability forced by seasonal winds that displace surface coastal water offshore. This process also supplies nutrients to the euphotic zone by Ekman transport and eventually supports phytoplankton blooms typically dominated by diatoms. Here, we investigate the relationship between biogenic silica production and mesoscale upwelling dynamics along the central region of the California Current System between 2013 and 2015, a period affected by a warm anomaly known as “the Blob.” Changes in the upwelling phenology along California caused by this marine heatwave are investigated using an innovative index and related to patterns of diatom production during upwelling events to evaluate diatom resilience. Based on this new index, we estimated that the nutrient supply to the euphotic zone declined by 50% during the Blob, but the Blob had little impact on local production during individual upwelling events. A statistical analysis evaluating the relationship between production and environmental conditions reveals persistent biological hotspots characterized by high biomass, depleted nutrients, and high specific production rates (up to  $0.7 \text{ d}^{-1}$ ) throughout the study period. Lower observed biogenic silica to Chlorophyll *a* ratios during the Blob suggested a taxonomic shift from siliceous to nonsiliceous phytoplankton and/or lightly silicified diatoms signaling a change at the base of the food chain that could have ramifications for productivity in this eastern boundary coastal upwelling system.

The development of an extraordinarily warm sea surface temperature anomaly along the west coast of North America ( $1\text{--}5^\circ\text{C}$  higher than average; Zaba and Rudnick 2016) called “the Blob” is now well documented. It developed near Alaska in the winter of 2013–2014, expanded southward to Baja California, and persisted throughout 2014 and 2015. The presence of the Blob altered several key physical ocean properties such as stratification, which led to a cascade of effects within the food web, including a decrease in total phytoplankton biomass and a shift in its community structure (e.g., Cavole

et al. 2016). This had substantial bottom-up implications that propagated through multiple trophic levels across the California Current System ecosystem. Although there have been studies of Blob’s impact on ocean biogeochemistry in the North Pacific (e.g., Bif et al. 2019), to our knowledge, and from a bottom-up forcing perspective, there are few, if any, studies addressing phytoplankton physiological tolerance or evolutionary adaptation to the Blob along the California Current System.

The California Current System is one of the several eastern boundary upwelling systems within the global ocean. A significant proportion of global primary production occurs in the coastal ocean with eastern boundary upwelling systems considered to be among the most productive ocean ecosystems (Mackas et al. 2006). The high productivity of eastern boundary upwelling systems is a result of wind-driven circulation processes that pulse nutrients into the surface ocean. Equatorward, Ekman transport driven by alongshore winds transports

\*Correspondence: ivia@ucsb.edu

This is an open access article under the terms of the Creative Commons Attribution-NonCommercial License, which permits use, distribution and reproduction in any medium, provided the original work is properly cited and is not used for commercial purposes.

Additional Supporting Information may be found in the online version of this article.

surface waters offshore which are replaced from below by the upwelling of cold, salty, and nutrient-rich water (Chavez and Messie 2009). In these systems, phytoplankton primary production supports a productive pelagic ecosystem with large population of fishes, seabirds, and marine mammals (Pauly and Christensen 1995). The enhancement of phytoplankton productivity and biomass by upwelling is especially pronounced when the upwelling event is followed by stratification and an optimal light environment (Largier et al. 2006). Understanding the drivers of seasonal and interannual changes in coastal upwelling intensity and frequency is important for evaluating their impacts on phytoplankton production and phytoplankton community structure in the future. Indeed, observational and modeling analysis shows that there has been an intensification of wind with global warming (e.g., Xiu et al. 2018). Increasing atmospheric temperatures cause continents to warm faster than oceans, and thus lead to more intense wind forced pressure gradients in coastal regions. This results in fewer, but longer, upwelling events over the course of the upwelling season (Bakun 1990). The likelihood and mechanisms underlying such a potential increase in upwelling favorable wind are still subject to debate (e.g., Sydesman et al. 2014; Rykaczewski et al. 2015). Model projections also agree that the upper ocean will become warmer and more stratified. As stratification develops, this will likely weaken upwelling (see Hsieh and Boer 1992) and lead to reduced nutrient fluxes to the upper ocean and a loss of production.

The California Current System extends from the North Pacific Current ( $\sim 50^\circ\text{N}$ ) to Baja California, Mexico ( $\sim 15\text{--}25^\circ\text{N}$ ), flowing toward the equator within about 100 km of the west coast of North America (Checkley Jr. and Barth 2009). The irregular coastline and bathymetry combined with temporal variations in external forcing result in a mosaic (in time and space) of ecosystems characterized by distinct hydrology and biogeochemistry. The most prominent physical forcing in the California Current System is the seasonal directional shift and/or intensification in winds that facilitate coastal upwelling. Upwelling events occur year-round along the California Current System, but they are most frequent during spring and occasional in summer (Bograd et al. 2009). Seasonal wind cycles generally lead to the highest levels of phytoplankton biomass and productivity in early spring, occasional high levels in summer and fall (Shipe and Brzezinski 2003), with peaks in offshore-transport that occur earlier in the south (April at  $33^\circ\text{N}$ ) than in the north (July at  $45^\circ\text{N}$ ). Changes in the intensity, amplitude, and phasing of seasonal upwelling events (phenology) critically affect the functioning of marine ecosystems in the California Current System from primary producers to top predators (e.g., Iles et al. 2012).

Upwelling driven phytoplankton blooms are initially dominated by diatoms (Lassiter et al. 2006) that are well adapted to exploit periods of high turbulence and high nutrient concentrations (Margalef 1978), making them more competitive during pulsed wind events when external “new” nutrients enter the

euphotic zone. Diatoms are important players in the carbon budgets of coastal upwelling regions and facilitate efficient transfer of energy to higher trophic levels (e.g., Verity et al. 1996). The prevalence and persistence of phytoplankton are linked to a myriad of biological, chemical, and physical factors, but diatoms are uniquely tied to the availability of silicon. Diatoms form their cell wall, called a frustule, by actively acquiring silicic acid (dissolved silicon) from the water and subsequently polymerizing the silicon as hydrated amorphous silica, or biogenic silica (hereafter  $\text{bSiO}_2$ ). The biological activity of diatoms can deplete upwelled silicic acid in a matter of days from 20 to  $30 \mu\text{mol L}^{-1}$  to concentrations that can limit the rate of  $\text{bSiO}_2$  production ( $\sim 2 \mu\text{mol L}^{-1}$ ; e.g., Krause et al. 2020) as well as growth rate ( $\sim 1 \mu\text{mol L}^{-1}$ ; e.g., Dugdale et al. 1995). The high productivity of diatoms ties silicon to the concentration, distribution, and fate of other biologically important elements like carbon, nitrogen, and iron. Additionally, the elemental stoichiometry of diatoms can differ depending on nutrient availability and can cause a preferential drawdown of one macronutrient over another (e.g., Si to N ratio; Brzezinski et al. 2002). Therefore, the degree to which silicic acid limits  $\text{bSiO}_2$  production has different implications for biogeochemical cycling and food web processes. Since macronutrient supply via Ekman transport regulates primary production in upwelling regions, silicon may at times play a central role in controlling diatom production and phytoplankton species succession within the California Current System.

Models of ocean productivity are not consistent in their predicted consequences of warming the surface ocean in coastal regions. Yet understanding the response of ecosystems to upwelling changes is critical for successful ecosystem-based management. Marine heat waves, such as the Blob, emulate a scenario of intense, temperature-driven, stratification in future ocean conditions. The immediate effect and the duration of effect of these warm water anomalies are still unclear. Here, we examine the changes in upwelling phenology during the Blob and use a compilation of biogeochemical measurements from three different cruises in the California Current System conducted from 2013 to 2015, during upwelling season, to investigate the interannual variability of diatom production associated with the Blob as a case study for the response to future climate.

## Materials and methods

### Sea surface temperature climatology and upwelling indices

Satellite data from NASA Giovanni (MODIS Aqua, <https://giovanni.gsfc.nasa.gov/giovanni/>) were compiled to examine sea surface temperatures along the coast of California and Oregon during July 2013, 2014, and May 2015 to align with the timing of oceanographic cruises in each of those years.

Long-term temporal trends in upwelling event frequency, duration, and strength based on the Coastal Upwelling Transport Index were used to detect changes in event-scale

upwelling and assess their ecological consequences. While similar to the well-known Bakun index, the Coastal Upwelling Transport Index uses a combination of Ekman and geostrophic transport to estimate the total volume of water upwelled or downwelled in a given time period, that is, the vertical volume transported into or out of the surface layer (units are volume of vertical transport per second per meter of coastline; Jacox et al. 2018). Positive Coastal Upwelling Transport Index values are the result of equatorward wind stress and imply upwelling, whereas negative values imply downwelling. Since upwelling has a cumulative effect on ecosystem productivity and structure, we focus on the Cumulative Upwelling Index which represents the summation of the daily upwelling indices at each location, starting on January 1<sup>st</sup> and continuing to the end of the year (see Bograd et al. 2009). The evolution of the Cumulative Upwelling Index over the course of an upwelling season reflects intraseasonal variations in upwelling intensity and can be used to discriminate upwelling events and wind relaxation.

Four additional indices were derived from the Cumulative Upwelling Index (as defined in Bograd et al. 2009): The start of the upwelling season (Spring Transition Index) is defined as the date when the climatological mean daily cumulative upwelling index first becomes positive (starts to increase). The end of the upwelling season is defined as the date when the climatological mean daily Cumulative Upwelling Index starts to decline. The Length of the Upwelling Season Index is defined as the number of days between the Spring Transition Index and the end of the upwelling season. Total upwelling magnitude index (TUMI) is the total volume of upwelled water over the course of the upwelling season.

Periodic reversals of upwelling-favorable winds, termed “wind relaxation,” break the upwelling season into a series of upwelling events. Some studies have shown that there is an optimal frequency of upwelling, relaxation, and stratification that promotes the dominance of diatoms (“optimal environmental window”; Wilkerson et al. 2006). In our case, we have classified upwelling events that last for at least 3 d and are followed by a relaxation period of at least 3 d as ecologically significant events optimal for diatom growth as suggested for the California Current System by Wilkerson et al. (2006).

The Biologically Effective Upwelling Transport Index (Jacox et al. 2018) estimates the total quantity of nitrate upwelled or downwelled in a given period of time (i.e., the vertical nutrient flux into or out of the mixed layer in  $\text{mmol NO}_3^- \text{ m}^{-1} \text{ s}^{-1}$ ) along the coastline. This nutrient-based index better captures bottom-up drivers of productivity in the California Current System since it quantifies not only the intensity of upwelling, but also the quality of upwelled waters in term of their nutrient content. To relate event-scale upwellings to diatom production regimes, a Silicic acid Upwelling Transport Index (in  $\text{mmol Si m}^{-1} \text{ s}^{-1}$ ) was calculated by multiplying the Biologically Effective Upwelling Transport Index with the Si : N ratio (using the average of silicic acid to nitrate plus nitrite ratios in subsurface

waters from the three cruises [approximately 1.15, note that nitrite concentrations are insignificant compared to nitrate concentrations; Supporting Information Fig. S1]).

### Sampling strategy and cruises description

This study leverages data from three cruises in the California Current System (Fig. 1) that measured diatom biomass (as  $\text{bSiO}_2$  concentration),  $\text{bSiO}_2$  production, the degree of silicon limitation, and macronutrient concentrations across a range of coastal upwelling and offshore waters. Because the same sampling strategy and sample processing were used among all cruises, all data are compared here to produce a compilation of environmental and biogeochemical parameters and diatom activity tracer measurements along the California Current System prior to and during the Blob event.

The “DYE labeling of diatom silica” DYEatom (PS1312) cruise aboard the R/V *Point Sur* in summer 2013 (27 June–05 July) sampled the central California coastline between Point Arena and Monterey Bay (from 36°N to 38°N) including two offshore stations. The IrnBru (MV1405) cruise aboard the R/V *Melville* in summer 2014 (04 July–21 July) sampled two transects off the California coast. The northern transect extended approximately 100 km southwest from Cape Blanco, Oregon, and the southern transect extended approximately 200 km west from Point Arena, California. The “Molecular Underpinnings of Silicification in the California Current” MUSiCC (OC1504A) cruise aboard the R/V *Oceanus* in spring 2015 (19 April–02 May) sampled inshore stations along the coast of California from Point Conception to Point Reyes and two stations off Oregon coastline (from 34°N to 44°N).

### Hydrological and biogeochemical parameters

For each cruise, regions of interest were defined using ocean color and sea surface temperatures (MODIS Level-2 product, NASA) in conjunction with surface currents available from High Frequency (HF) radar arrays to target upwelling plume or phytoplankton biomass hotspots.

During the IrnBru cruise, two transects were designed to follow the trajectory of a cold plume of upwelled water as it was advected offshore. A suite of environmental measurements such as sea surface temperatures and salinity were taken in a both a discrete and continuous manner along both transects. Seawater was collected in the upper 5 m using Niskin bottles or a towed trace metal clean surface pump (see Bruland et al. 2005). Samples for nitrate and orthophosphate concentrations were filtered through 0.6  $\mu\text{m}$  polycarbonate membrane filters and measured onboard using a Lachat flow injection analysis system (Parsons et al. 1984). Biogenic silica and silicic acid were measured on the particulate and filtrate material after filtration through a 1.2  $\mu\text{m}$  polycarbonate membrane using the colorimetric ammonium molybdate method for silicic acid (Brzezinski and Nelson 1995) and a sodium hydroxide digestion method for  $\text{bSiO}_2$  (Krause et al. 2009). Chlorophyll *a* (Chl *a*) was filtered through a cellulose membrane and measured using a 90% acetone extraction

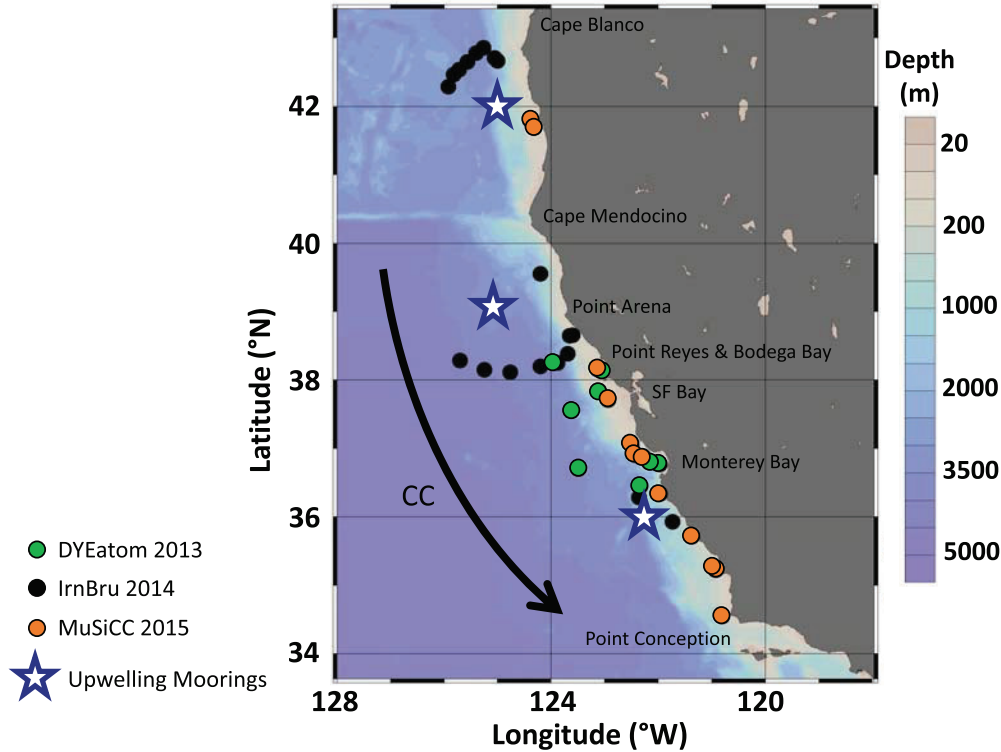


**Fig. 1.** Station map of the three cruises along the California Coast. The location of the recurrent upwelling centers (stars) with moorings used for calculation of the upwelling indices (see text). CC refers to the general southward flow of the California Current.

and acidification technique (Brzezinski and Washburn 2011). More information about sampling during the IrnBru cruise is detailed in McNair et al. (2018a,b).

During the DYEatom and MUSiCC cruises, seawater was sampled using a CTD-rosette system equipped with twelve 10-liter Niskin bottles, a fluorometer, and a photosynthetically active radiation sensor. The intensity of the photosynthetically active radiation just below the surface ( $I_0$ ) was used to determine the depths at which the photosynthetically active radiation was 55%, 22%, 7%, and 1% of  $I_0$  and 55%, 36%, 14%, 5%, and 1% for DYEatom and MUSiCC, respectively. Macronutrients were measured at these depths for all stations. Water for inorganic nutrients was syringe filtered through a 0.6  $\mu\text{m}$  polycarbonate filter into plastic vials and immediately frozen. On shore, nutrients were quantified using a Lachat flow injection system (Parsons et al. 1984). Chl *a* was measured using the same technique as for IrnBru. Biogenic silica samples were filtered through a 1.2  $\mu\text{m}$  polycarbonate filter, immediately frozen, and analyzed later using a sodium hydroxide digestion method (Krause et al. 2009). More information about sampling during the DYEatom cruise is detailed elsewhere (Kranzler et al. 2019; Krause et al. 2020).

### Production rate measurements

Biogenic silica production rates were measured from the three cruises following the same procedure as described in Krause et al. (2011). During the IrnBru transects, seawater was

collected between 2 and 5 m at each station, spiked with a solution of the radioisotope  $^{32}\text{Si}$  and incubated in deck-board, flow-through incubators for 24 h. The 24 h incubation time ensured samples experienced equal length of light and dark despite differences in starting times. 261 Bq of  $^{32}\text{Si}$  was added to samples from the northern transect and 293 Bq of  $^{32}\text{Si}$  was added to samples from the southern transect. During DYEatom and MUSiCC, seawater was collected using Niskin bottles at each depth and 260 Bq of  $^{32}\text{Si}$  was added to the samples. Following isotope addition, bottles were placed for 24, 12, or 4 h in deck-board incubators simulating the light level at the depth of collection.

Following incubation, samples were filtered through 1.2  $\mu\text{m}$  polycarbonate membranes, mounted on nylon planchettes, air-dried, and covered with Mylar film. Biogenic silica production rates were determined by measuring  $^{32}\text{Si}$  activity using low-level beta detection and after aging samples into secular equilibrium between  $^{32}\text{Si}$  and  $^{32}\text{P}$ ,  $\sim 120$  d (Krause et al. 2011). Gross biogenic silica production rates, or  $\text{bSiO}_2$  production rates ( $\mu\text{mol Si L}^{-1} \text{d}^{-1}$ ), were normalized to  $\text{bSiO}_2$  concentration to determine specific rates ( $\text{d}^{-1}$ ) as in Brzezinski and Phillips (1997). Depth-integrated values of these parameters have been calculated using the standard trapezoidal integration method.

### Statistical analysis

In order to investigate the response of diatoms to local upwelling events along the California Current System,

physical parameters (such as temperature and salinity), nutrients (silicic acid, nitrate, and phosphate concentrations), biomass proxies (bSiO<sub>2</sub> and Chl *a* concentrations), and biological rates measured in surface water at all stations during the three cruises were combined in a principal component analysis. This analysis was performed using the package “FactoMineR” and plots generated using “ggplot2” in the software R.

Variables were selected to be included in the principal component analysis in an iterative fashion based on their squared coefficient of correlation (cos<sup>2</sup>) with the axis or dimension, that is, the proportion of the variance of the variables explained by the axis. Factors with cos<sup>2</sup> greater than 0.5 for at least one dimension were included in the principal component analysis. For dimension 1 (*y*-axis), nutrients (silicic acid, nitrate, and phosphate) are the variables that are best represented by the axis with a cos<sup>2</sup> of 0.89, 0.96, and 0.95, respectively. For dimension 2 (*x*-axis), bSiO<sub>2</sub>, Chl *a*, temperature, and salinity are the variables that have the highest cos<sup>2</sup> (0.81, 0.74, 0.76, and 0.67, respectively).

## Results

### Sensitivity of the California Current Ecosystem to climate forcing

#### Changes in sea surface temperature and Chl *a*

The sea surface temperature data from July 2014 and 2015, after the arrival of the Blob, showed that both offshore and coastal waters from Point Conception (36°N) to Point Arena (39°N) had warmed compared to July 2013 (Supporting Information Fig. S2). The active upwelling region extended from north of Point Conception (34°N) to Point Reyes (38°N) during the 2013 (DYEatom) and 2015 (MUSiCC) cruises and was more confined inshore and to the north of Point Reyes during the 2014 (IrnBru) cruise (Fig. 2). Generally, Chl *a* accumulation occurred downstream from the upwelling center along each upwelling plume. This observation is common in most coastal upwelling systems and is clearly seen during DYEatom and IrnBru cruises with downstream high-chlorophyll waters being confined nearshore south of the upwelling centers or in eddies, and filaments of cold water (see Fig. 2).

#### Changes in upwelling phenology

The main physical effect of the Blob was a change in the amplitude and phasing of seasonal upwelling and relaxation events (phenology). Prior to the Blob, in 2013, the Cumulative Upwelling Index shows the typical latitudinal gradient of the onset and intensity of upwelling along the California Current System (Table 1). At 42°N, the upwelling season started in spring and continued through the fall while it spanned almost the full year at 36°N (Table 1). Among all latitudes, there is evidence of a seasonal cycle of Ekman transport; prior to the Blob, the spring transition occurs earlier in the south (36°N, Early February) than in the north (42°N, Late March). The timing of the onset and duration of the upwelling season changed with the Blob (2014–2015) with a delayed spring

transition and earlier endings of the upwelling season at all latitudes. This resulted in upwelling seasons that were 50% (2014) and 72% (2015) shorter than the average duration characteristic of pre-Blob years (1967–2007 and 2013; Table 1). The upwelling intensity declined drastically during the Blob (TUMI is between 46% and 36% lower in 2014 and 2015, respectively, compared to pre-Blob 2013 conditions), indicating a lower seasonal supply of new nutrients to the surface during the Blob. Finally, there was a decline in the number of ecologically significant alternations between upwelling and relaxation events (or optimal windows) critical for the development of phytoplankton from 2013 to 2015 (Table 1; Fig. 3).

#### Influence on productivity drivers: Si supply

Alteration of the upwelling season along the California Current System during the Blob critically impacts productivity drivers such as the supply of nutrients (including Si) into the euphotic zone. The Silicic acid Upwelling Transport Index (mmol Si m<sup>-1</sup> s<sup>-1</sup>) is an estimate of the rate of total silicic acid upwelled or downwelled within 30 km of the coastline and can be converted into a mean annual Si supply (in mol Si m<sup>-2</sup> yr<sup>-1</sup>). Daily values of the Silicic acid Upwelling Transport Index (Supporting Information Fig. S3) indicate a latitudinal variation in the seasonal cycles of Si supply along the California Current System, even during Blob conditions, with the highest wind-driven Si supply around 39°N and the lowest at 36°N (Table 2). At all latitudes, we observed a drastic drop (around 50%) in the Si supply via Ekman transport during the Blob conditions in 2014 and 2015.

#### Observations during oceanographic cruises

##### Silicic acid drawdown, biogenic silica accumulation, and production rates

Prior to the Blob (during DYEatom, 2013), samples collected at multiple offshore and coastal stations near Monterey Bay and Point Reyes show significant silicic acid drawdown in surface waters (Fig. 4a). Biogenic silica accumulation (∫bSiO<sub>2</sub>, integrated over the euphotic zone) was lower offshore (< 33 mmol m<sup>-2</sup>) compared to coastal stations (42–327 mmol m<sup>-2</sup>) and ranged from 81.7 to 188.1 mmol m<sup>-2</sup>, and 154.5 to 327.4 mmol m<sup>-2</sup> in Monterey Bay and Point Reyes domains, respectively (Table 3). Biogenic silica concentration maxima in most profiles were at, or near, the surface with the highest concentration observed in the Point Reyes domain. Rates of bSiO<sub>2</sub> production were highly variable among the different domains, but generally declined rapidly with depth to values near analytical zero at the base of the euphotic zone (Fig. 4a). Integrated bSiO<sub>2</sub> production rate was lower offshore compared to coastal stations which ranged from 11.0 to 42.1 mmol m<sup>-2</sup> d<sup>-1</sup> and 8.0 to 22.6 mmol m<sup>-2</sup> d<sup>-1</sup> in Monterey Bay and Point Reyes, respectively (Table 3).

During the first year of the Blob (IrnBru, 2014), stations along the two transects were spread across the trajectory of upwelled water as cold water was flowing offshore (Fig. 2).

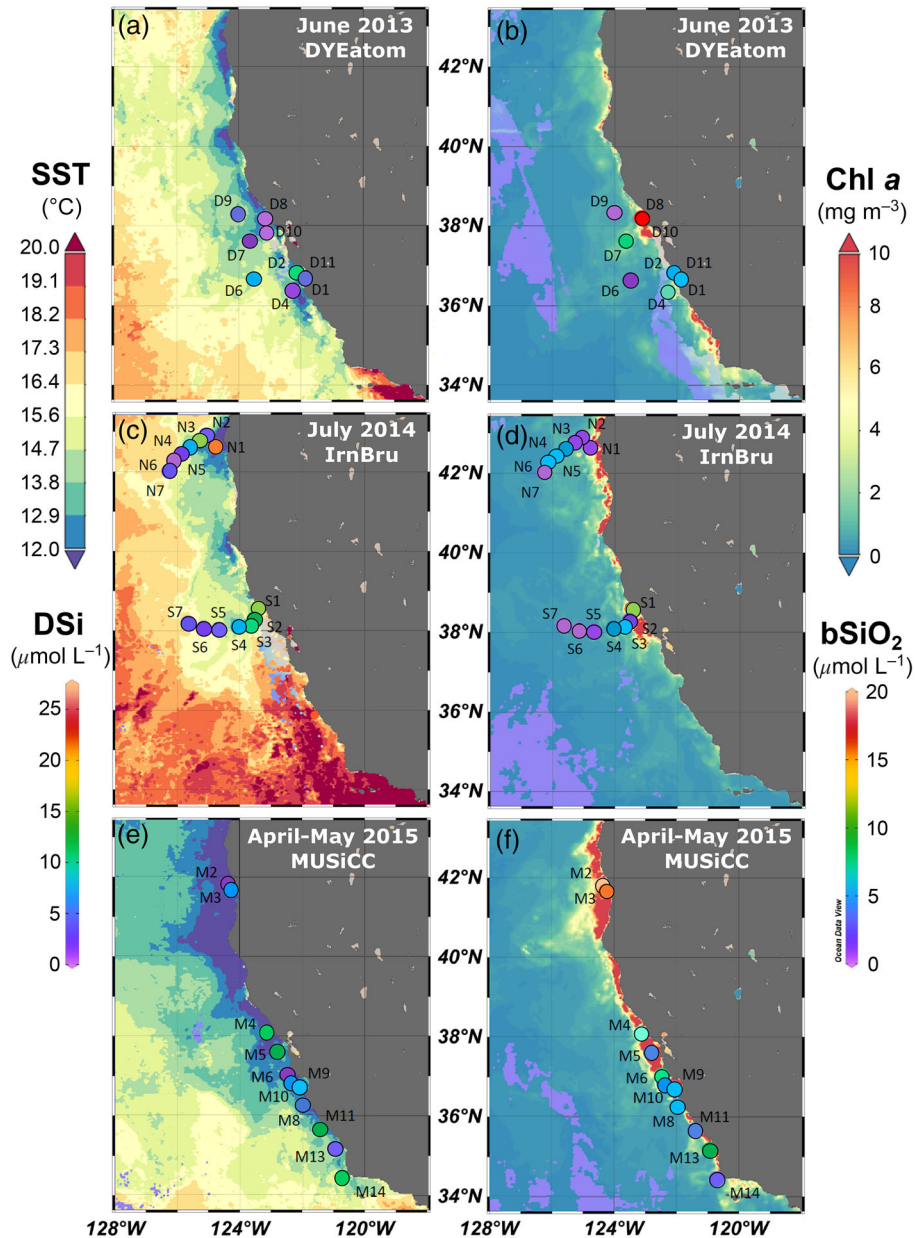


**Fig. 2.** The California Current System during the DYEatom (July 2013; **a, b**), IrnBru (July 2014; **c, d**), and MUSiCC (May 2015; **e, f**) cruises. Panels (**a**), (**c**), and (**e**) display sea surface temperature (SST, surface colors, °C), along with silicic acid concentration (DSi, circles,  $\mu\text{mol L}^{-1}$ ). Panels (**b**), (**d**), and (**f**) display surface-water distribution of Chl *a* concentration (surface colors,  $\text{mg m}^{-3}$ ) along with biogenic silica concentration ( $\text{bSiO}_2$ , circles,  $\mu\text{mol L}^{-1}$ ). Satellite data is adapted from NASA Giovanni (MODIS Aqua, <https://giovanni.gsfc.nasa.gov/giovanni/>).

Surface silicic acid concentration ranged from 0.7 to  $21.2 \mu\text{mol L}^{-1}$  and from 2.6 to  $15.4 \mu\text{mol L}^{-1}$  along the northern and southern transect, respectively (Fig. 5). Silicic acid was highly coupled with nitrate and phosphate with all three nutrients decreasing in concentration away from shore (see McNair et al. 2018a for more details). Biogenic silica concentration displayed a different pattern along each transect (Figs. 2d, 5), increasing along the northern transect from  $0.9 \mu\text{mol L}^{-1}$  nearshore (Sta. N1) to  $5.5 \mu\text{mol L}^{-1}$  offshore (Sta.

N6), but decreasing away from shore along the southern transect from  $10.6 \mu\text{mol L}^{-1}$  (Sta. S1) to  $0.06 \mu\text{mol L}^{-1}$  (Sta. S7). Biogenic silica production rates fluctuated across the transects from 0.01 to  $11.53 \mu\text{mol L}^{-1} \text{d}^{-1}$  and generally increased with increasing  $\text{bSiO}_2$  (Fig. 5). Specific  $\text{bSiO}_2$  production rates were higher nearshore in both transects and ranged from 0.10 to  $0.86 \text{d}^{-1}$  (see McNair et al. 2018a for more details). Note that, the specific  $\text{bSiO}_2$  production rate is normalized to the standing stock of  $\text{bSiO}_2$  which includes

**Table 1.** Comparison of the phenology of the upwelling season between the years of the current study and pre-Blob period. Optimal window is the number of events combining at least 3 days of upwelling followed by at least three relaxation days (numbers in parenthesis for this parameter are optimal windows outside of the upwelling season).

		Pre-Blob		Blob	
		1967–2007*	2013	2014	2015
42°N	STI	Late March	09 Apr	15 May	14 Apr
	END	Late October	24 Dec	20 Sep	02 Nov
	LUSI (days)	223±37	259	128	202
	TUMI ( $\text{m}^3 \text{s}^{-1} \text{m}^{-1}$ )	191±73	242	155	189
	Optimal windows		9 (2)	1 (0)	6 (3)
39°N	STI	Late February	04 Jan	10 Mar	19 Feb
	END	Late November	20 Dec	19 Nov	01 Dec
	LUSI (days)	282±45	350	254	285
	TUMI ( $\text{m}^3 \text{s}^{-1} \text{m}^{-1}$ )	294±98	315	202	237
	Optimal windows		5 (2)	3 (1)	2 (1)
36°N	STI	Early February	02 Jan	14 Apr	15 Mar
	END	Late December	26 Dec	03 Dec	31 Dec
	LUSI (days)	320±37	358	233	291
	TUMI ( $\text{m}^3 \text{s}^{-1} \text{m}^{-1}$ )	278±60	289	154	221
	Optimal windows		4 (2)	2 (1)	2 (1)

END, end of the upwelling season; LUSI, length of the upwelling season index; STI, spring transition index; TUMI, total upwelling magnitude index.  
\*Mean and standard deviation from Bograd et al. (2009).

silica in both living cells and detritus. The presence of this nonactive pool of  $\text{bSiO}_2$  means that the specific  $\text{bSiO}_2$  production rate underestimates the  $\text{bSiO}_2$  production rate of living cells. This is especially true at the end of both transects where the nonactive pool of  $\text{bSiO}_2$  was a significant fraction of the total  $\text{bSiO}_2$  (e.g., up to 90% at the farthest offshore station of the southern transect; McNair et al. 2018b).

During the second year of the Blob (MUSiCC, 2015), samples were collected at several coastal stations but no significant geographic pattern was apparent in any of the key parameters (Fig. 4b). The northernmost stations off Oregon exhibited the highest silicic acid drawdown (surface concentration  $< 1.5 \mu\text{mol L}^{-1}$ ) and highest  $\text{bSiO}_2$  accumulation in the euphotic zone ( $\int \text{bSiO}_2 = 159.2 \text{ mmol m}^{-2}$ , with surface concentration as high as  $19.6 \mu\text{mol L}^{-1}$ , see Fig. 4b and Table 3). For all other stations, there was a clear silicic acid drawdown in the euphotic zone except for Sta. M1, M4, M5, and M14. Biogenic silica concentrations were homogenous within the euphotic zone at each station and ranged from  $2.4$  to  $8.8 \mu\text{mol L}^{-1}$ . Integrated biogenic silica stocks ranged from  $41.8$  to  $128.0 \text{ mmol m}^{-2}$  and were not as variable as during DYEatom (Table 3). Biogenic silica production rates were generally maximal in the surface, ranging from  $1.6$  to  $3.9 \mu\text{mol L}^{-1} \text{d}^{-1}$  except for Sta. M4 and M13 where the maximum (up to  $5.7 \mu\text{mol L}^{-1} \text{d}^{-1}$ ) was in the subsurface (Fig. 4b). Integrated biogenic silica production rates ranged from  $13.3 \text{ mmol m}^{-2} \text{d}^{-1}$  south of Point Sur to  $61.2 \text{ mmol m}^{-2} \text{d}^{-1}$  between Point Sur and Point Reyes (Table 3).

### Biogenic silica to Chl *a* ratios

Although it has been debated in the marine science community, measures of Chl *a* concentration have been widely used as a metric for phytoplankton biomass. Chl *a* is the most practical and extensively used proxy of phytoplankton biomass over large spatial scale because it explains much of the variance in marine primary production and can capture first order changes in phytoplankton biomass (e.g., Boyce et al. 2014). Because diatoms have an obligate requirement for silicic acid and are the dominant group of siliceous plankton in surface waters of coastal upwelling ecosystems, the ratio  $\text{bSiO}_2:\text{Chl } a$  can be used as a proxy of (1) the contribution of diatoms to the phytoplankton community and (2) variations in physiology within a diatom assemblage (Fig. 6).

Biogenic silica to Chl *a* ratios varied among coastal features that influence upwelling and the retention of upwelled waters. Alongshore variability in the California Current System is driven by interaction of currents with bathymetric features such as coastal headlands and embayments that generate regions of less intense upwelling, or “shadow zones,” which could serve as retentive regions for marine organisms (e.g., Graham and Largier 1997). Two types of environments were sampled across the three cruises, distinct upwelling centers that supported high phytoplankton biomass (group 1) and those located in a retention/shadow zone (group 2; e.g., Monterey Bay). Prior to the Blob (DYEatom, 2013), the  $\text{bSiO}_2 : \text{Chl } a$  was distinct between these two environments with higher  $\text{bSiO}_2 : \text{Chl } a$  for stations from the upwelling

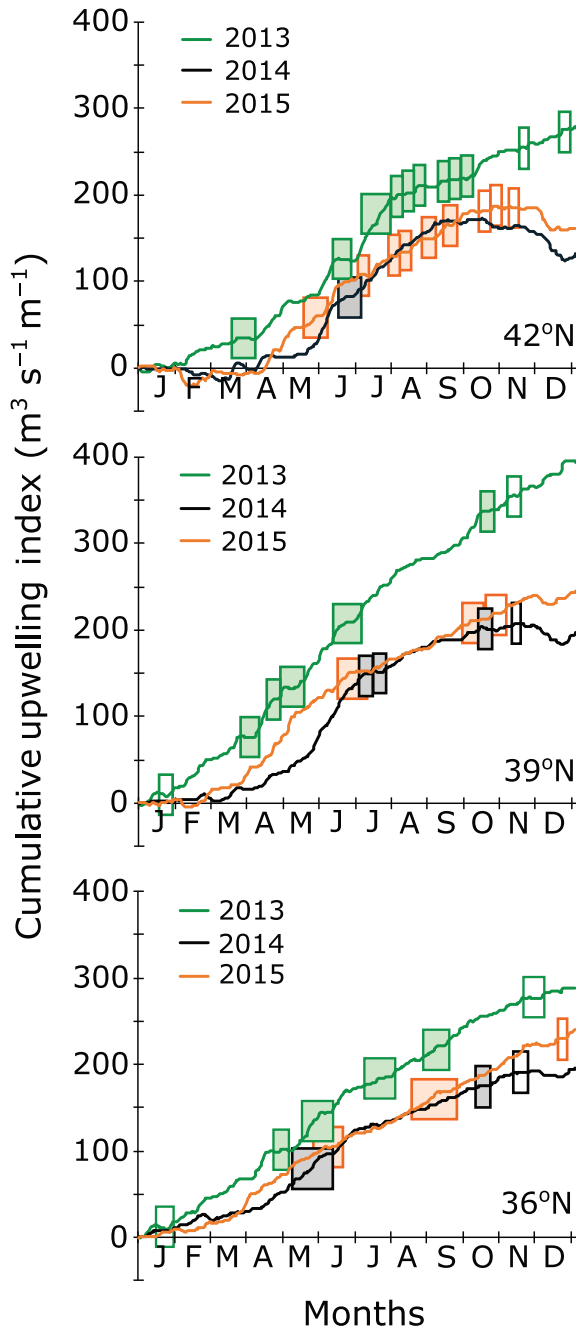


**Fig. 3.** Seasonal variability of the cumulative upwelling index. Shaded boxes are the optimal windows for diatom growth as defined by at least 3 days of upwelling followed by three relaxation days. Open boxes are optimal windows outside of the upwelling season (see text).

group ( $bSiO_2 : Chl\ a$  ratio  $129.2 \pm 9.0$ ,  $R^2 = 0.88$ ; Fig. 6) compared to that of the retention zone ( $bSiO_2 : Chl\ a$  ratio  $21.1 \pm 4.7$ ,  $R^2 = 0.50$ ; Fig. 6). In contrast, during the Blob (IrnBru, 2014 and MUSiCC, 2015), overall  $bSiO_2 : Chl\ a$  ratios were similar between the two environments and more closely resembled the low values found in retention zones during

**Table 2.** Si flux into the mixed layer along the California Current System calculated from SiUTI: Silicic acid upwelling transport index.  $\int SiUTI$  is the summation of the daily SiUTI at each location; Si supply is the mean annual Si supply estimated from  $\int SiUTI$  and integrated within the 30 km of coastline used to defined SiUTI;  $\Delta SiUTI$  is the Si supply change (in %) relative to nonblob conditions (2013).

		2013	2014	2015
42°N	$\int SiUTI$ ( $mmol\ m^{-1}\ s^{-1}$ )	4556.47	2451.69	2299.62
	Si supply ( $mol\ m^{-2}\ yr^{-1}$ )	13.12	7.06	6.62
	$\Delta SiUTI$ (%)	0	-46	-50
39°N	$\int SiUTI$ ( $mmol\ m^{-1}\ s^{-1}$ )	7045.85	3370.32	3303.35
	Si supply ( $mol\ m^{-2}\ yr^{-1}$ )	20.29	9.71	9.51
	$\Delta SiUTI$ (%)	0	-52	-53
36°N	$\int SiUTI$ ( $mmol\ m^{-1}\ s^{-1}$ )	3858.85	1687.71	1472.82
	Si supply ( $mol\ m^{-2}\ yr^{-1}$ )	11.11	4.86	4.24
	$\Delta SiUTI$ (%)	0	-56	-62

nonblob conditions ( $24.6 \pm 6.1$  and  $24.3 \pm 1.2$ ,  $R^2 = 0.57$  and  $0.89$  for IrnBru and MUSiCC, respectively).

#### Drivers of variability

Most of the spatial and temporal variability observed (up to 73%) can be explained along the two main axes of the principal component analysis (Fig. 7), controlled by an inverse relationship between nutrients and biomass proxies (axis 1) and a second inverse relationship between temperature and salinity (axis 2). Those relationships define a gradient from inshore (cold and nutrient replete newly upwelled waters) to offshore (warm and nutrient depleted aged upwelled waters). As expected, stations from the two IrnBru transects (2014), along with the two offshore DYEatom stations (2013), sit along this diagonal gradient. All DYEatom (non-Blob conditions) and MUSiCC (Blob conditions) stations were randomly distributed along both axes of the principal component analysis; however, they do not sit along the upwelled water gradient on the principal component analysis. Instead they fall in a region characterized by higher biomass accumulation ( $bSiO_2$  and  $Chl\ a$ ), homogeneous hydrological conditions (temperature and salinity), and variable nutrient concentrations (silicic acid, nitrate, and phosphate).

## Discussion

### Sensitivity of the California Current Ecosystem to climate forcing

#### Upwelling changes associated with the Blob

During our 2014 and 2015 field observations, an anomalously warm water mass was present within the California Current System. Our analysis of changes in upwelling phenology showed that the main physical effect of the Blob was fewer, less intense, upwelling events over a shorter upwelling season. This led to less frequent and shorter optimal condition



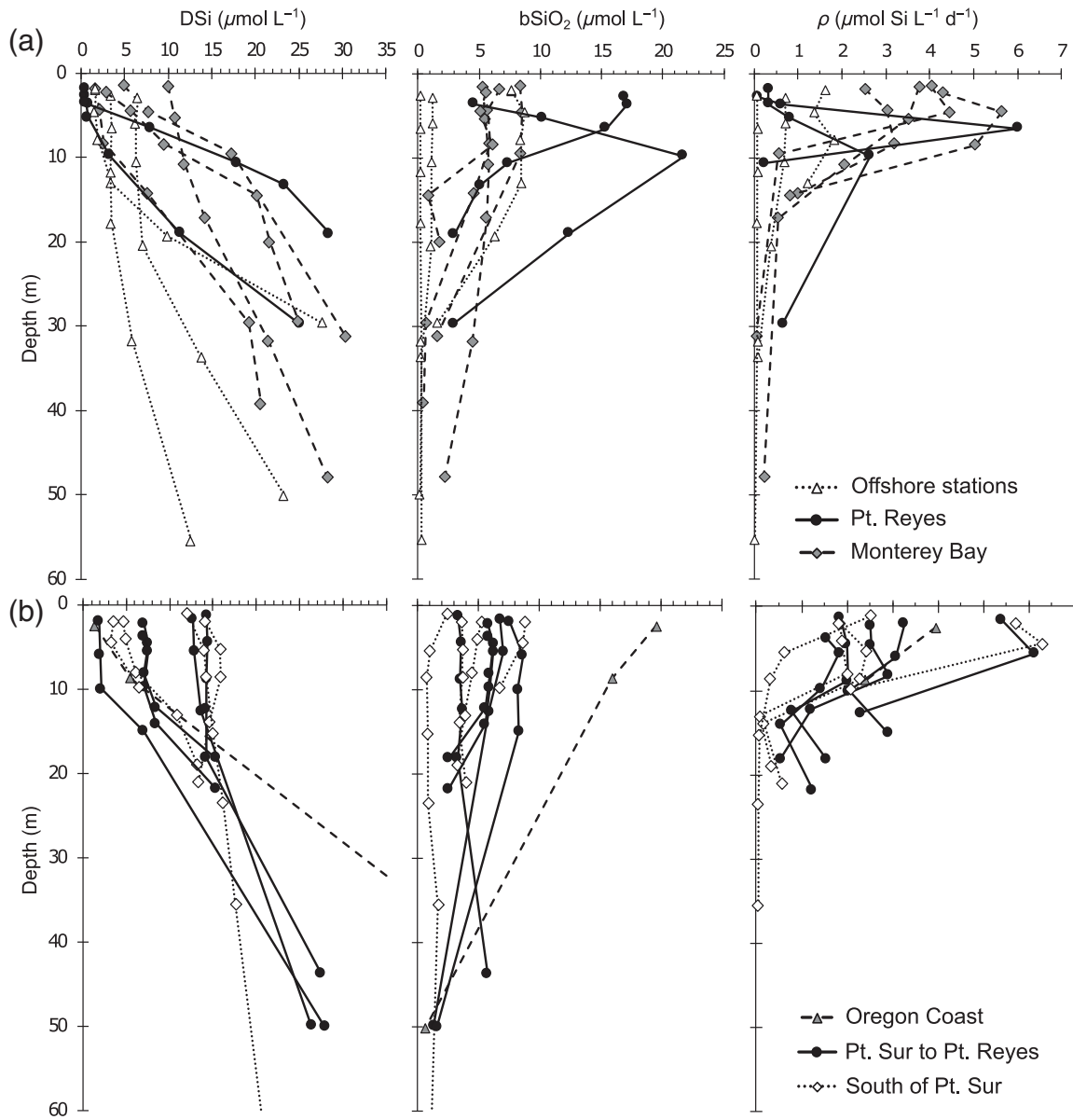


**Fig. 4.** Profiles of silicic acid concentration (DSi,  $\mu\text{mol L}^{-1}$ ), biogenic silica (bSiO<sub>2</sub>,  $\mu\text{mol L}^{-1}$ ), and bSiO<sub>2</sub> production rate ( $\rho$ ,  $\mu\text{mol Si L}^{-1} \text{d}^{-1}$ ) during the DYEatom (2013, **a**) and MUSiCC (2015, **b**) cruises.

windows for diatom blooms (Fig. 3; Table 1), as well as a drastic drop (around 50%) of the annual silicic acid supply to the mixed layer via Ekman transport that persisted throughout the Blob (Table 2).

The total amount of nutrients delivered to the ocean surface by upwelling, and therefore potential diatom production, depends on the volume and nutrient content of upwelled water. The total volume of upwelled water, inferred from TUMI, is driven largely by the strength of the equatorward winds that drive offshore Ekman transport. During the Blob, TUMI declined drastically between 46% and 36% lower in 2014 compared to pre-Blob 2013 conditions and did not fully recover in 2015

(TUMI between 22% and 25% lower compared to 2013). Therefore, variations of TUMI can alone explain most of the decrease in silicic acid supply observed during the Blob. However, nutrient concentrations in upwelled waters also depend on upwelling source depth. When coastal waters are strongly stratified, the source waters for onshore flow come from shallower depths (e.g., Lentz and Chapman 2004). Shallower source waters usually have lower nutrient content, contributing to reduced silicic acid flux into the mixed layer. Fewer upwelling events (or optimal windows) and warmer sea surface temperatures would likely lead to stronger stratification and shallower mixed layer depth amplifying the effect of a reduced TUMI.

**Table 3.** Biogenic silica concentration ( $\int bSiO_2$ ) and  $bSiO_2$  production rates ( $\int \rho$ ) integrated over the euphotic layer, measured during the DYEatom (2013) and MUSiCC (2015) cruises. Ze represents the bottom of the euphotic zone (1% of surface Photosynthetically Active Radiation [PAR]).

	Station	Latitude	Longitude	Sector	Ze (m)	$\int bSi$ ( $mmol\ m^{-2}$ )	$\int \rho$ ( $mmol\ Si\ m^{-2}\ d^{-1}$ )	
DYEatom	1	36°46.86'N	121°59.12'W	Monterey Bay	31	188.15	37.99	
	2	36°48.47'N	122°10.84'W	Monterey Bay	17	95.52	42.08	
	4	36°27.31'N	122°20.32'W	Monterey Bay	14	81.73	22.86	
	6	36°42.61'N	123°29.62'W	Offshore	34	32.67	11.42	
	7	37°33.42'N	123°37.96'W	Pt. Reyes	13	108.23	20.07	
	8	38°8.96'N	123°5.95'W	Pt. Reyes	11	154.51	22.60	
	9	38°15.89'N	123°58.12'W	Offshore	55	14.11	2.86	
	10	37°50.24'N	123°6.60'W	Pt. Reyes	30	327.42	8.00	
	11	36°46.67'N	121°58.83'W	Monterey Bay	29	126.00	11	
	MUSiCC	2	41°47.92'N	124°23.44'W	Oregon Coast	9	159.24	29.56
		4	38°9.44'N	123°7.23'W	Pt. Sur to Pt. Reyes	13	84.17	61.22
5		37°42.98'N	122°56.34'W	Pt. Sur to Pt. Reyes	18	64.15	28.87	
6		37°3.95'N	122°30.16'W	Pt. Sur to Pt. Reyes	16	127.99	42.99	
8		36°20.5'N	121°58.77'W	South of Pt. Sur	20	83.18	20.87	
9		36°53.35'N	122°17.09'W	Pt. Sur to Pt. Reyes	18	96.42	34.86	
10		36°54.95'N	122°25.28'W	Pt. Sur to Pt. Reyes	22	105.53	26.81	
11		35°43.06'N	121°22.64'W	South of Pt. Sur	21	77.32	27.57	
13		35°13.95'N	120°55.72'W	South of Pt. Sur	10	80.70	48.61	
14		34°33.06'N	120°48.74'W	South of Pt. Sur	35	41.79	13.34	

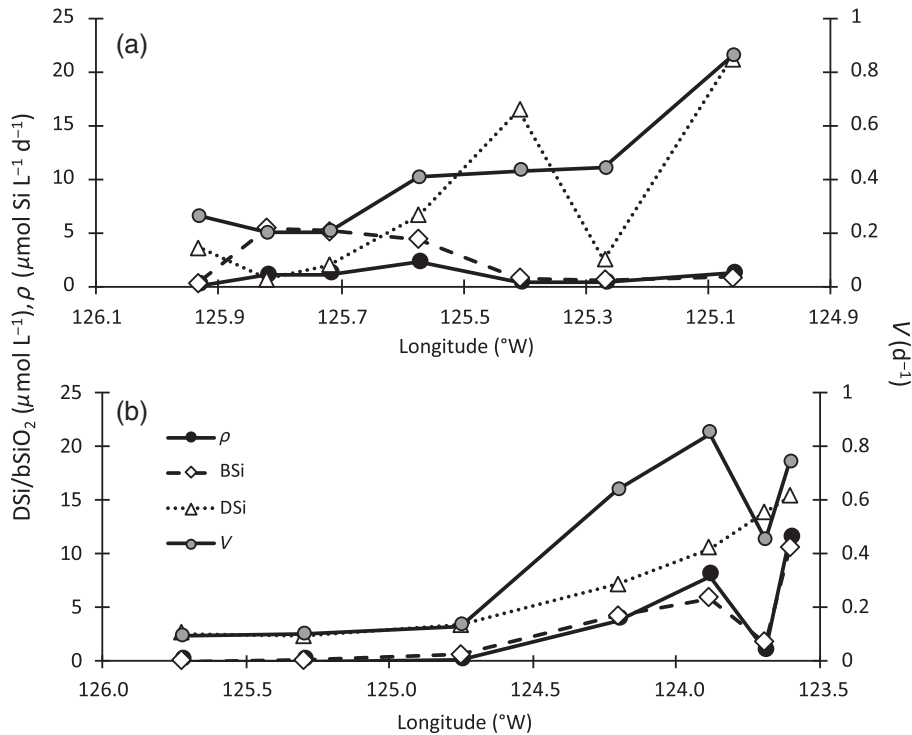


**Fig. 5.** Concentration of silicic acid (silicic acid,  $\mu mol\ L^{-1}$ ) and biogenic silica ( $bSiO_2$ ,  $\mu mol\ L^{-1}$ ), along with  $bSiO_2$  production rate ( $\rho$ ,  $\mu mol\ Si\ L^{-1}\ d^{-1}$ ) and specific  $bSiO_2$  production rate ( $V$ ,  $d^{-1}$ ) across the northern (a) and southern (b) transects of IrnBru cruise (2014).

**Biological response to the Blob**

Several hypotheses can explain a decreasing  $bSiO_2 : Chl a$  in the bulk particulate matter between upwelling and

retention zones and between non-Blob (DYEatom, 2013) and Blob (IrnBru and MUSiCC, 2014 and 2015) conditions:

- i. An increase of the detrital pool of diatom silica or differential recycling of organic matter and  $bSiO_2$  would lead to increased  $bSiO_2 : Chl a$ . Mortality by grazing or viral lysis would lead to an increase in the detrital pool of  $bSiO_2$ , while enhanced bacterial activity would lead to preferential degradation of organic matter (including pigments) over  $bSiO_2$  dissolution in surface waters. Enhanced bacterial activity has been observed during diatom bloom demise when the particulate pool is mostly composed of empty frustules (Smith et al. 1995). Indeed, during DYEatom (2013), stations in the Pt. Reyes domain (higher  $bSiO_2 : Chl a$ ) were characterized by high bacterial ectoprotease activity associated with the recent lysis of the diatom population by viral infection (Kranzler et al. 2019), while Monterey Bay stations (lower  $bSiO_2 : Chl a$ ), were characterized by a high abundance of cell-associated diatom viruses suggesting an active, early stage of infection in which the population had not yet lysed.
- ii. A switch of phytoplankton communities from siliceous to nonsiliceous organisms would lower  $bSiO_2 : Chl a$ . For example, warm stratified conditions are generally considered favorable for motile dinoflagellates (Margalef 1978)

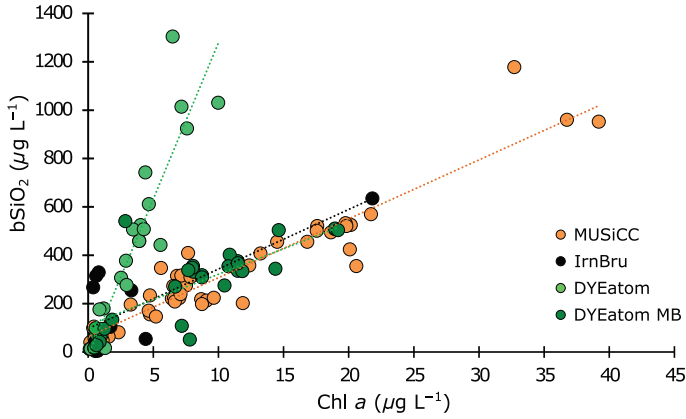


**Fig. 6.** Temporal and spatial evolution of the  $bSiO_2 : Chl a$  relationship between Blob and non-Blob conditions for the three cruises (DYEatom, 2013; IrnBru, 2014; and MUSiCC, 2015) and between Monterey Bay stations and other stations during DYEatom (dark vs. light green dots). Biogenic silica was converted from molar to mass unit by using the atomic mass of Si (28.1 u). Line represents the linear regression for IrnBru (black,  $R^2 = 0.57$ ), DYEatom (light green,  $R^2 = 0.88$ ), DYEatom Monterey Bay (dark green,  $R^2 = 0.50$ ), and MUSiCC (orange,  $R^2 = 0.89$ ).

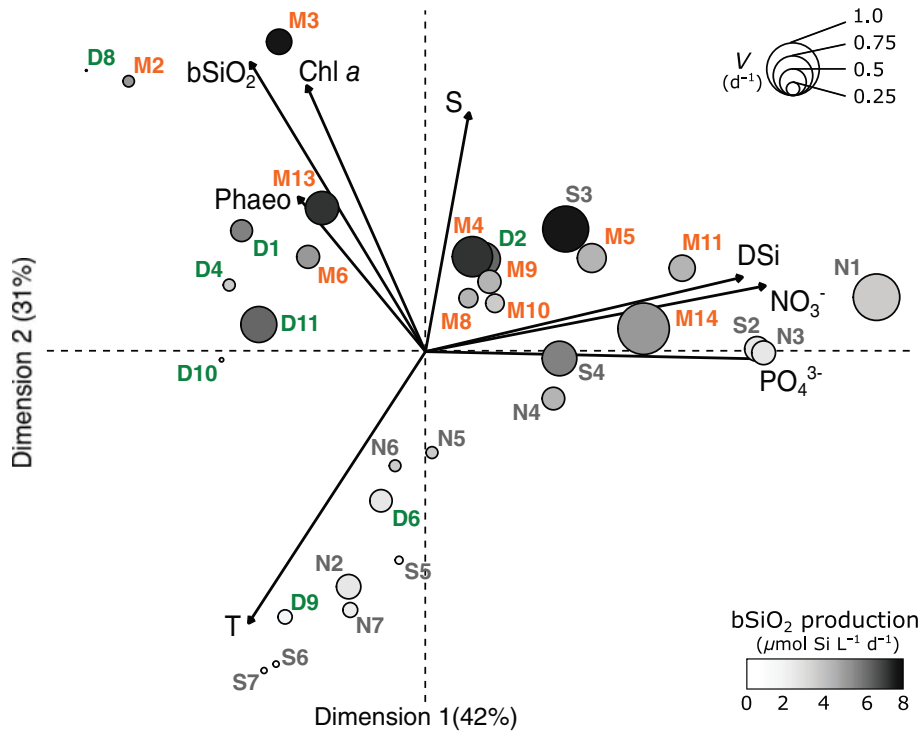


**Fig. 7.** Principal component analysis of DYEatom (2013, green labels), IrnBru (2014, gray labels) and MUSiCC (2015, orange labels) surface samples showing the rate of  $bSiO_2$  production ( $\rho, \mu mol Si L^{-1}$ , gray scale bar) and the specific  $bSiO_2$  production rate ( $V, d^{-1}$ , sizes). Forty-two percentage of the variability is explained by the inverse relationship between nutrients (silicic acid, nitrate, and phosphate, all in  $\mu mol L^{-1}$ ) and biomass proxies ( $bSiO_2$  in  $\mu mol L^{-1}$ ;  $Chl a$  and pheopigments, both in  $\mu g L^{-1}$ ) on the x-axis; and 31% of the variability is explained by the inverse relationship between salinity (S) and temperature (T,  $^{\circ}C$ ) on the y-axis.

that can access nutrients within and below a shallow thermocline. One scenario is that diatoms dominate turbulent waters rich in nutrients during nonblob conditions (DYEatom), while dinoflagellates constitute the bulk of the community in stratified water typical of retention zones or during Blob conditions (IrnBru and MUSiCC). However, stations from Monterey Bay (i.e., retention zones) during DYEatom were characterized by diatom-dominated 18S ribosomal RNA reads and enriched diatom transcript abundance (Kranzler et al. 2019; Krause et al. 2020), indicating an abundant and active diatom community. Thus, a more likely explanation for the decrease in  $\text{bSiO}_2$  : Chl *a* is a shift within the diatom community to less silicified genera. Indeed, Monterey Bay was dominated by the genus *Pseudo-nitzschia* which is less silicified than the *Chaetoceros* and *Thalassiosira* genera (McNair et al. 2018a) that were associated with upwelling events (Kranzler et al. 2019). During Blob conditions, the lower  $\text{bSiO}_2$  : Chl *a* we observed is consistent with reports of an extensive coastwide bloom of the toxigenic *Pseudo-nitzschia australis* (McCabe et al. 2016) initiated during the Blob in 2015.

- iii. Although a taxonomic shift in the diatom community could lead to lower  $\text{bSiO}_2$  : Chl *a*, a change in diatom physiology could also lower  $\text{bSiO}_2$  : Chl *a*. Diatoms are known to decouple silica production and growth rates and can adjust cellular silicon quota depending on the biogeochemical conditions they encounter. For example, cultured and in situ diatoms decrease silicification under severe silicon limitation to maintain maximum growth rates (i.e., McNair et al. 2018a). On the other hand, growth limitation by other factors (light, iron, nitrate, etc.) often inversely correlate with silicification because a decrease in growth slows cell cycle progression allowing cells more time to acquire silicon and results in a fully silicified cell even when silicic acid is low (Claquin et al. 2002).

It is likely that the particular biogeochemical conditions that characterize the Blob would have induced a progressive shift in the community composition. Studies have shown that the taxonomic composition of phytoplankton communities is closely linked with oceanic circulation and mesoscale physical processes (i.e., Edwards and Richardson 2004). These processes influence the flux of essential nutrients from the subsurface nutrient pool into the euphotic layer, which can affect phytoplankton physiology. Along the California Current System, the physical processes leading to water column stratification associated with the Blob could lead to alterations in diatom physiology, or select for nonsiliceous organisms, such as motile dinoflagellates that prefer calm conditions associated with stratified waters or less silicified diatoms species.

#### **Diatoms' resilience to climate forcing in the CCS Biogenic silica production across the upwelling plume**

The idealized response of phytoplankton to upwelling productivity cycle has been described as a succession of physiological

states occurring along a conveyor belt (Dugdale et al. 1990) and can be observed in the principal component analysis. First, phytoplankton cells with low biological rates due to low light conditions were carried to the surface; Chl *a* concentrations were low and concentrations of nutrient were high (e.g., Sta. N1–N3 and S2). Then, as the water was advected offshore, diatoms experienced an energy shift-up in the high-irradiance, high nutrient surface environment, that is, they turned on nutrient-uptake mechanisms and started to photosynthesize (Kudela et al. 1997). Nutrient uptake was initially low but increased rapidly, resulting in a drawdown of nutrients to near detection limits (e.g., Sta. S3, S4, and N4). Further offshore, diatoms run out of nutrients, rate processes were slowed, and there was a switch to dominance by the microbial loop and smaller phytoplankton that use regenerated nutrients (e.g., Sta. N5–N7 and S5–S7). Eventually, biological particles were exported below the euphotic layer or recycled. It has been thought that typically, the cycle from upwelling to nutrient depletion takes about 5–7 d (Dugdale et al. 1990).

Interestingly here, despite the consumption of nutrients, biomass did not increase offshore in either transect during IrnBru in 2014. High production associated with the upwelling plume could be consumed by grazers or exported below the euphotic zone via sinking or subduction of surface waters (e.g., Bograd and Mantyla 2005). Those processes can easily explain the lack of biomass accumulation. However, they fail to explain the low specific  $\text{bSiO}_2$  production rates observed offshore on both transects. In addition to the influence of detrital material (nonliving diatom silica, e.g., grazed fragments), one hypothesis could be the redistribution of biomass via horizontal transport or advection. Indeed, the California Current System consists of a system of filamented currents or jets meandering between mesoscale eddies (15–30 km in diameter). This highly dynamic system can change substantially on a weekly time scale and provides a mechanism for rapid (a few days) transport of nutrients and biota associated with coastal upwelling (e.g., Mooers and Robinson 1984). In this scenario, diatoms will consume nutrients in the upwelling plume and be horizontally advected toward regions where hydrological conditions allow their accumulation in the euphotic zone. Those regions, also called retention zones, represent hot spots for plankton biomass accumulation and export, and are key components of the carbon and silicon pump on the coastal shelf (e.g., Stukel et al. 2017). This hypothesis is consistent with models indicating a decoupling between new and export production along the Central California coast due to the transport of small particles associated with mesoscale phenomena (e.g., Plattner et al. 2005).

Alteration of diatom physiology is likely to be reflected in the  $\text{bSiO}_2$  production rates which will provide a mechanistic understanding of diatom resilience and their ability to dominate phytoplankton communities during large-scale climate forcing scenarios. When combining all stations together in the principal component analysis (Fig. 7), we did not observe

any specific trend or systematic difference in bSiO<sub>2</sub> production rates between individual upwelling events, with the exception of two stations located in the north (Sta. M2 and M3) that displayed low temperature, low nutrient, high biomass accumulation, and where production was likely controlled by a different wind-driven upwelling regime compared to the other stations. All DYEatom (non-Blob conditions) and MUSiCC (Blob conditions) stations were randomly distributed along both axes of the principal component analysis, suggesting diatoms can use adaptive strategies (e.g., physiological adjustments; McNair et al. 2018a and reference therein) to maintain growth and bloom even in drastically changing surface ocean conditions such as a marine heat wave. In this situation, diatom activity and biomass accumulation would be maintained at the scale of an upwelling event and depend only on the supply of silicic acid into the euphotic zone. Therefore, variations in regional cumulative bSiO<sub>2</sub> production will likely be the result of changes in upwelling phenology rather than alterations in the local rate of biological production.

#### Retention zones vs. upwelling plumes

Retentive region stations can be identified on Fig. 7 as the group of stations characterized by warmer temperatures, higher salinities, low nutrient concentrations, and moderate to high Chl *a* and bSiO<sub>2</sub> production rates (e.g., silicic acid < 7 μmol L<sup>-1</sup>, bSiO<sub>2</sub> > 4 μmol L<sup>-1</sup>, and bSiO<sub>2</sub> production rates > 1.5 μmol Si L<sup>-1</sup> d<sup>-1</sup>; Sta. D1, D2 and D11 and Sta. M8, M9, M10 and M13 from DYEatom and MUSiCC cruises, respectively). Most of these stations are located in Monterey Bay, a key region for coastal production known for having both upwelling and retention zones that act as a refuge for many populations including zooplankton, mammals, and fisheries (Kudela et al. 2008). This combination creates a favorable environment for diatom growth. Indeed, this alternation between pulse nutrient supply via upwelling and stratification during relaxation events, or within retention zones, is thought to be the primary physical driver for the success of diatoms in the highly productive eastern boundary upwelling ecosystems. Wilkerson et al. (2006), working on the Point Arena–Point Reyes region, suggest that a 3–7 d relaxation following an upwelling pulse is optimal for phytoplankton (and especially diatoms) to bloom. A corollary of that time dependence is that biomass accumulation will be observed 3–7 d after an upwelling event in calm locations downstream of source waters, as in the retention zones (see also Vander Woude et al. 2006). These retention zones play a quantitative role in the carbon sequestration on the shelf as well as source regions of various organic and inorganic materials for the adjacent open ocean (e.g., Pilskaln et al. 1996). Together, the inability to distinguish diatom production rates between Blob and non-Blob years, and the persistent decrease in production along an upwelling path (either offshore or into a retention zone) suggest that diatom production rates are more strongly influenced by immediate, daily scale.

#### Conclusion

As coastal upwelling is driven by large-scale regional atmospheric patterns, global climate change has the potential to affect physical and ecological processes through changes in water chemistry and water temperature. By affecting water temperature, nutrient availability, and phytoplankton productivity, changes in the duration, frequency, and magnitude of upwelling are likely to significantly impact the structure and functioning of coastal ecosystems in eastern boundary upwelling ecosystems around the world.

The results presented here suggest that total diatom net bSiO<sub>2</sub> production along the California Current System was likely reduced by 50% during an anomalous warm event called the Blob. Increased stratification from the Blob decreased strength and frequency of upwelling in the California Current during the 2014 spring, and led to a reduction of 50% of the silicic acid supply into the euphotic zone. In the future, additional increased solar heating may enhance stratification to a point when upwelling would only turnover water from shallower horizon, bringing less nutrient-rich deep water to the surface.

Diatom production rates within local blooms were not significantly different between the three upwelling seasons suggesting little effect of the Blob on the local intensity of individual productivity events. However, bSiO<sub>2</sub> : Chl *a* ratios imply that phytoplankton communities during the Blob were likely dominated by nonsiliceous organisms. The change in the phytoplankton community implies a shift at the base of the food chain with ramifications for the productivity of the coastal ecosystem. Warming events like that of 2014 are predicted to become more common as the climate warms (Oliver et al. 2018). The results presented here connect warming events to fundamental changes of the structure of a biologically productive and economically important ecosystem. The Blob was indeed associated with a variety of unusual biological events and species sightings and caused economic losses due to the reduction in the abundance of prey available for commercially valuable species (Cavole et al. 2016). Associated ecosystem impacts also include an unprecedented harmful algal bloom, primarily the diatom *Pseudo-nitzschia* sp., ranging from Alaska to southern California by July, resulting in the closure of many fisheries along the U.S. West Coast and impacting many species of marine mammals (McCabe et al. 2016).

Our results offer insights into the likely impacts of future warming on phytoplankton dynamics and improve our understanding, in a bottom-up perspective, of impacts of marine extreme events such as the Blob on marine ecosystem functioning and ecosystem services. Although the 2013–2015 warm water anomaly may be an imperfect predictor of what the future may hold, many of the biological and physical shifts observed during the Blob could happen more frequently in the context of the global climate change. Extreme positive sea surface temperature anomalies over much of the northeast Pacific are already happening in 2019–2020 and might lead to

a new marine heat wave along the coast of California. It is thus critical to develop more consistent understanding of the relationships between phytoplankton, nutrients, and upwelling that can be used to understand and forecast the variability in the primary production along the California Current System and design appropriate management strategies in a future where the phytoplankton communities will be less frequently dominated by diatoms.

Combining climate forcing indices developed from long-term data series with local and direct sampling of biogeochemical parameters and processes across a defined region allows us to better estimate the response of phytoplankton communities to climate change. This could be assessed through a more systematic survey of the local phytoplankton communities and their biogeochemical dynamic, and/or through the development of new indices that will record more directly the response of phytoplankton communities to future climate forcing, and that are not limited to the description of biogeochemical and physical changes in the ecosystems.

## References

- Bakun, A. 1990. Global climate change and intensification of coastal ocean upwelling. *Science* **247**: 198–201. doi:10.1126/science.247.4939.198
- Bif, M. B., L. Siqueira, and D. A. Hansell. 2019. Warm events induce loss of resilience in organic carbon production in the northeast Pacific Ocean. *Global Biogeochem. Cycles* **33**: 1174–1186. doi:10.1029/2019GB006327
- Bograd, S. J., and A. W. Mantyla. 2005. On the subduction of upwelled waters in the California Current. *J. Mar. Res.* **63**: 863–885. doi:10.1357/002224005774464229
- Bograd, S. J., I. Schroeder, N. Sarkar, X. Qiu, W. J. Sydeman, and F. B. Schwing. 2009. Phenology of coastal upwelling in the California Current. *Geophys. Res. Lett.* **36**: L01602. doi:10.1029/2008GL035933
- Boyce, D. G., M. Dowd, M. R. Lewis, and B. Worm. 2014. Estimating global chlorophyll changes over the past century. *Prog. Oceanogr.* **122**: 163–173. doi:10.1016/j.pocean.2014.01.004
- Bruland, K. W., E. L. Rue, G. J. Smith, and G. R. DiTullio. 2005. Iron, macronutrients and diatom blooms in the Peru upwelling regime: Brown and blue waters of Peru. *Mar. Chem.* **93**: 81–103. doi:10.1016/j.marchem.2004.06.011
- Brzezinski, M. A., and D. M. Nelson. 1995. The annual silica cycle in the Sargasso Sea near Bermuda. *Deep-Sea Res. Part I Oceanogr. Res. Pap.* **42**: 1215–1237. doi:10.1016/0967-0637(95)93592-3
- Brzezinski, M. A., and D. R. Phillips. 1997. Evaluation of  $^{32}\text{Si}$  as a tracer for measuring silica production rates in marine waters. *Limnol. Oceanogr.* **45**: 856–865. doi:10.4319/lo.1997.42.5.0856
- Brzezinski, M. A., and others. 2002. A switch from  $\text{Si}(\text{OH})_4$  to  $\text{NO}_3^-$  depletion in the glacial Southern Ocean. *Geophys. Res. Lett.* **29**(12): 1–4. doi:10.1029/2001GL014349
- Brzezinski, M. A., and L. Washburn. 2011. Phytoplankton primary productivity in the Santa Barbara Channel: Effects of wind-driven upwelling and mesoscale eddies. *J. Geophys. Res. Oceans* **116**: C12013. doi:10.1029/2011JC007397
- Cavole, L. M., and others. 2016. Biological impacts of the 2013–2015 warm water anomaly in the Northeast Pacific: Winners, losers, and the future. *Oceanography* **29**: 273–285. doi:10.5670/oceanog.2016.32
- Chavez, F. P., and M. Messie. 2009. A comparison of eastern boundary upwelling ecosystems. *Prog. Oceanogr.* **83**: 80–96. doi:10.1016/j.pocean.2009.07.032
- Checkley, D. M., Jr., and J. A. Barth. 2009. Patterns and processes in the California Current System. *Prog. Oceanogr.* **83**: 49–64. doi:10.1016/j.pocean.2009.07.028
- Claquin, P., V. Martin-Jézéquel, J. C. Kromkamp, M. J. W. Veldhuis, and G. W. Kraay. 2002. Uncoupling of silicon compared with carbon and nitrogen cultures of *Thalassiosira pseudonana* (Bacillariophyceae) under light, nitrogen, and phosphorus control. *J. Phycol.* **38**: 922–930. doi:10.1046/j.1529-8817.2002.t01-1-01220.x
- Dugdale, R. C., F. P. Wilkerson, and A. Morel. 1990. Realization of new production in coastal upwelling areas: A means to compare relative performance. *Limnol. Oceanogr.* **35**: 822–829. doi:10.4319/lo.1990.35.4.0822
- Dugdale, R. C., F. P. Wilkerson, and H. J. Minas. 1995. The role of silicate pump in driving the new production. *Deep-Sea Res. Part I Oceanogr. Res. Pap.* **42**: 697–719.
- Edwards, M., and A. J. Richardson. 2004. Impact of climate change on marine pelagic phenology and trophic mismatch. *Nature* **430**: 881–884. doi:10.1038/nature02808
- Graham, W. M., and J. L. Largier. 1997. Upwelling shadows as nearshore retention sites: The example of northern Monterey Bay. *Cont. Shelf Res.* **17**: 509–532. doi:10.1016/S0278-4343(96)00045-3
- Hsieh, W. W., and G. J. Boer. 1992. Global climate change and ocean upwelling. *Fish. Oceanogr.* **1**: 333–338. doi:10.1111/j.1365-2419.1992.tb00005.x
- Iles, A. C., T. C. Gouhier, B. A. Menge, J. S. Stewart, A. J. Haupt, and M. Lynch. 2012. Climate-driven trends and ecological implications of event-scale upwelling in the California Current System. *Glob. Chang. Biol.* **18**: 783–796. doi:10.1111/j.1365-2486.2011.02567.x
- Jacox, M. G., C. A. Edwards, E. L. Hazen, and S. J. Bograd. 2018. Coastal upwelling revisited: Ekman, Bakun, and improved upwelling indices for the U.S. West Coast. *J. Geophys. Res. Oceans* **123**: 7332–7350. doi:10.1029/2018JC014187
- Kranzler, C. F., and others. 2019. Silicon limitation facilitates virus infection and mortality of marine diatoms. *Nat. Microbiol.* **4**: 1790–1797. doi:10.1038/s41564-019-0502-x

- Krause, J. W., D. M. Nelson, and M. W. Lomas. 2009. Biogeochemical responses to late-winter storms in the Sargasso Sea II: Increased rates of biogenic silica production and export. *Deep-Sea Res. Part I Oceanogr. Res. Pap.* **56**: 861–874. doi:10.1016/j.dsr.2009.01.002
- Krause, J. W., M. A. Brzezinski, and J. L. Jones. 2011. Application of low-level beta counting of  $^{32}\text{Si}$  for the measurement of silica production rates in aquatic environments. *Mar. Chem.* **127**: 40–47. doi:10.1016/j.marchem.2011.07.001
- Krause, J. W., M. A. Brzezinski, J. L. Largier, H. M. McNair, M. Maniscalco, K. D. Bidle, A. E. Allen, and K. Thamatrakoln. 2020. The interaction of physical and biological factors drives phytoplankton spatial distribution in the northern California Current. *Limnol. Oceanogr.* **9999**: 1–16. doi:10.1002/lno.11431
- Kudela, R. M., W. P. Cochlan, and R. C. Dugdale. 1997. Carbon and nitrogen uptake response to light by phytoplankton during an upwelling event. *J. Plankton Res.* **19**: 609–630. doi:10.1093/plankt/19.5.609
- Kudela, R. M., and others. 2008. New insights into the controls and mechanisms of plankton productivity along the US West Coast. *Oceanography* **21**: 46–59. <https://www.jstor.org/stable/24860007>
- Largier, J. L., and others. 2006. WEST: A northern California study of the role of wind-driven transport in the productivity of coastal plankton communities. *Deep-Sea Res. Part II Top. Stud. Oceanogr.* **53**: 2833–2849. doi:10.1016/j.dsr2.2006.08.018
- Lassiter, A. M., F. P. Wilkerson, R. C. Dugdale, and V. E. Hogue. 2006. Phytoplankton assemblages in the CoOP-WEST coastal upwelling area. *Deep-Sea Res. Part II Top. Stud. Oceanogr.* **53**: 3063–3077. doi:10.1016/j.dsr2.2006.07.013
- Lentz, S. J., and D. C. Chapman. 2004. The importance of nonlinear cross-shelf momentum flux during wind-driven coastal upwelling. *J. Phys. Oceanogr.* **34**: 2444–2457. doi:10.1175/JPO2644.1
- Mackas, D. L., P. T. Strub, A. Thomas, and V. Montecino. 2006. Eastern regional ocean boundaries pan-regional overview, p. 21–60. *In* A. R. Robinson and K. Brink [eds.], *The sea*, 14A ed. Harvard Univ. Press.
- Margalef, R. 1978. Life-forms of phytoplankton as survival alternatives in an unstable environment. *Oceanol. Acta* **134**: 493–509.
- McCabe, R. M., and others. 2016. An unprecedented coastwide toxic algal bloom linked to anomalous ocean conditions. *Geophys. Res. Lett.* **43**: 10366–10376. doi:10.1002/2016GL070023
- McNair, H. M., M. A. Brzezinski, and J. W. Krause. 2018a. Diatom populations in an upwelling environment decrease silica content to avoid growth limitation. *Environ. Microbiol.* **20**: 4184–4193. doi:10.1146/annurev.marine.010908.163650
- McNair, H. M., M. A. Brzezinski, C. P. Till, and J. W. Krause. 2018b. Taxon-specific contributions to silica production in natural diatom assemblages. *Limnol. Oceanogr.* **63**: 1056–1075. doi:10.1002/lno.10754
- Mooers, C. N. K., and A. R. Robinson. 1984. Turbulent jets and eddies in the California Current and inferred cross-shore transports. *Science* **223**: 51–53. doi:10.1126/science.223.4631.51
- Oliver, E. C. J., and others. 2018. Longer and more frequent marine heatwaves over the past century. *Nat. Commun.* **9**: 1324. doi:10.1038/s41467-018-03732-9
- Parsons, T., Y. Maita, and C. Lalli. 1984. *A manual of chemical and biological methods for seawater analysis*. Pergamon Press.
- Pauly, D., and V. Christensen. 1995. Primary production required to sustain global fisheries. *Nature* **374**: 255–257.
- Piaskaln, C. H., J. B. Paduan, F. P. Chavez, R. Y. Anderson, and W. M. Berelson. 1996. Carbon export and regeneration in the coastal upwelling system of Monterey Bay, Central California. *J. Mar. Res.* **54**: 1149–1178. doi:10.1357/0022240963213772
- Plattner, G.-K., N. Gruber, H. Frenzel, and J. C. McWilliams. 2005. Decoupling marine export production from new production. *Geophys. Res. Lett.* **32**: L11612. doi:10.1029/2005GL022660
- Rykaczewski, R. R., J. P. Dunne, W. J. Sydeman, M. Garcia-Reyes, B. A. Black, and S. J. Bograd. 2015. Poleward displacement of coastal upwelling-favorable winds in the ocean's eastern boundary currents through the 21<sup>st</sup> century: Upwelling responses to climate change. *Geophys. Res. Lett.* **42**: 6424–6431. doi:10.1002/2015GL064694
- Shipe, R. F., and M. A. Brzezinski. 2003. Siliceous plankton dominate primary and new productivity during the onset of El Niño conditions in the Santa Barbara Basin, California. *J. Mar. Syst.* **42**: 127–143. doi:10.1016/S0924-7963(03)00071-X
- Smith, D. C., G. F. Steward, R. A. Long, and F. Azam. 1995. Bacterial mediation of carbon fluxes during a diatom bloom in a mesocosm. *Deep-Sea Res. Part II Top. Stud. Oceanogr.* **42**: 75–97. doi:10.1016/0967-0645(95)00005-B
- Stukel, M. R., and others. 2017. Mesoscale ocean fronts enhance carbon export due to gravitational sinking and subduction. *Proc. Natl. Acad. Sci. USA* **114**: 1252–1257. doi:10.1073/pnas.1609435114
- Sydeman, W. J., M. Garcia-Reyes, D. S. Schoeman, R. R. Rykaczewski, S. A. Thompson, B. A. Black, and S. J. Bograd. 2014. Climate change and wind intensification in coastal upwelling ecosystems. *Science* **345**: 77–80. doi:10.1126/science.1251635
- Vander Woude, A. J., J. L. Largier, and R. M. Kudela. 2006. Nearshore retention of upwelled waters north and south of Point Reyes (northern California) – patterns of surface temperature and chlorophyll observed in CoOP WEST. *Deep-*

- Sea Res. Part II Top. Stud. Oceanogr. **53**: 2985–2998. doi:[10.1016/j.dsr.2006.07.003](https://doi.org/10.1016/j.dsr.2006.07.003)
- Verity, P. G., D. K. Stoecker, M. E. Sieracki, and J. R. Nelson. 1996. Microzooplankton grazing of primary production at 140°W in the equatorial Pacific. Deep-Sea Res. Part II Top. Stud. Oceanogr. **43**: 1227–1255. doi:[10.1016/0967-0645\(96\)00021-5](https://doi.org/10.1016/0967-0645(96)00021-5)
- Wilkerson, F. P., A. M. Lassiter, R. C. Dugdale, A. Marchi, and V. E. Hogue. 2006. The phytoplankton bloom response to wind events and upwelled nutrients during the CoOP WEST study. Deep-Sea Res. Part II Top. Stud. Oceanogr. **53**: 3023–3048. doi:[10.1016/j.dsr2.2006.07.007](https://doi.org/10.1016/j.dsr2.2006.07.007)
- Xiu, P., F. Chai, E. N. Curchitser, and F. S. Castruccio. 2018. Future changes in coastal upwelling ecosystems with global warming: The case of the California Current System. Sci. Rep. **8**: 2866. doi:[10.1038/s41598-018-21247-7](https://doi.org/10.1038/s41598-018-21247-7)
- Zaba, K. D., and D. L. Rudnick. 2016. The 2014–2015 warming anomaly in the Southern California Current System observed by underwater gliders. Geophys. Res. Lett. **43**: 1241–1248. doi:[10.1002/2015GL067550](https://doi.org/10.1002/2015GL067550)

### Acknowledgments

The authors gratefully thank the Captains and crews of the R/V *Pt. Sur*, R/V *Melville*, and R/V *Oceanus* as well as Marine Technicians for their dedication and invaluable assistance in sample collection. The authors are especially grateful to T. Coale and K. Bruland for providing nitrate and phosphate data for IrnBru, M. Maniscalco, and I. Marquez for assistance with silica production rates measurements during cruises, and L. Washburn for enlightening advise concerning upwelling indices. This work was supported by grants from the National Science Foundation (OCE-1155663 to J.W.K.; OCE-1333929 to K.T.; OCE-1334387 to M.A.B.). The three cruise data sets are available from the Biological and Chemical Oceanography Data Management Office under Project numbers 550825 and 558198.

### Conflict of Interest

None declared.

Submitted 28 May 2020

Revised 25 September 2020

Accepted 21 November 2020

Associate editor: Heidi Sosik